

The GIRAFFE Inner Bulge Survey (GIBS)

Manuela Zoccali^{1,2}
 Oscar A. Gonzalez³
 Sergio Vasquez^{1,2}
 Vanessa Hill⁴
 Marina Rejkuba^{3,5}
 Elena Valenti³
 Alvio Renzini⁶
 Alvaro Rojas-Arriagada⁴
 Carine Babusiaux⁷
 Tom Brown⁸
 Dante Minniti^{2,9,10}
 Andy McWilliam¹¹

¹ Instituto de Astrofísica, Pontificia Universidad Católica de Chile, Santiago, Chile

² The Millennium Institute of Astrophysics, Chile

³ ESO

⁴ Université de Nice Sophia Antipolis, CNRS, France

⁵ Excellence Cluster Universe, Garching, Germany

⁶ INAF-Osservatorio di Padova, Italy

⁷ GEPI, Observatoire de Paris, France

⁸ Space Telescope Science Institute, Baltimore, USA

⁹ Departamento de Ciencias Físicas, Universidad Andres Bello, Chile

¹⁰ Vatican Observatory, Italy

¹¹ Carnegie Institute of Washington, Pasadena, USA

The GIRAFFE Inner Bulge Survey (GIBS) is a spectroscopic survey of ~ 6500 core helium burning (red clump) stars in the Milky Way Bulge, carried out with the FLAMES GIRAFFE spectrograph at the VLT. The aim of the GIBS survey is to derive the metallicity and radial velocity distributions of Bulge stars, across 31 fields in the region of Galactic longitude range -10° to $+10^\circ$ and latitude range -10° to $+5^\circ$. This is the area also mapped by the VISTA Variables in the *Via Láctea* (VVV) ESO Public Survey.

With a mass $\sim 10^{10} M_\odot$ in stars, the Galactic Bulge is the only bulge in which we can resolve individual stars down to the bottom of the main sequence. It is also the only bulge for which high-resolution spectra can be obtained for giant stars, providing chemical abundances of several atomic species. Nevertheless,

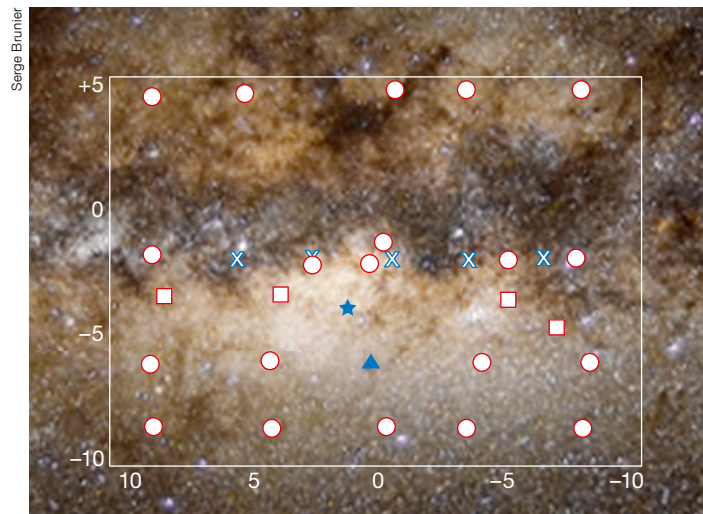


Figure 1. Approximate location of the observed fields, overlaid on an optical image of the Milky Way Bulge. The large white rectangle is the area covered by the VVV survey. Open circles are fields observed at $R \sim 6500$ in the CaT spectral region (LR8), while open squares are fields observed at $R \sim 22\,500$ around ~ 6300 Å (HR13). Crosses are fields observed in LR8 in programme 89.B-0830. The blue star is the field, in Baade's Window, used for the CaT calibration and the blue triangle is the field discussed in Vásquez et al. (2013).

due to the high level of crowding, absolute and differential interstellar extinction, and foreground disc contamination, our knowledge of the Bulge structure, kinematics and stellar population is still relatively poor. The ultimate goal, when studying the Galactic Bulge, is to set constraints on the formation mechanism(s) of the Milky Way and, by extension, of galaxies in general.

The inner region (< 3 kpc) of the Milky Way has been known for a long time to host a bar (Blitz & Spergel, 1991). Only recently, however, have detailed 3D maps been constructed using red clump stars as distance indicators; these maps have revealed that the outer Bulge exhibits a strong boxy/peanut component, sometimes also called X-shaped (e.g., McWilliam & Zoccali, 2010). Dynamical models predict the formation of boxy/peanut structures as the outcome of the secular evolution of a disc, through the formation and subsequent vertical heating of a bar. Observationally, these models are confirmed by the cylindrical rotation of the Bulge (Howard et al., 2009) and by the asymmetries in the radial motions of the near and far edges of the Bar (Vásquez et al., 2013). We might conclude, therefore, that we understand the Bulge structure, kinematics and formation mechanism, except that several other observations indicate the presence of at least another component in the Bulge. The metal-poor component of the Bulge has spheroid-like kinematics and high α -element to iron ratios $[\alpha/\text{Fe}]$, while

the metal-rich component has kinematics more typical of a bar, and relatively low $[\alpha/\text{Fe}]$ (e.g., Hill et al., 2011). Moreover, when tracing the 3D structure of the Bulge using RR Lyrae variables, which are clean tracers of the oldest stellar population, a spheroidal structure is found, with no evidence of either a bar or a boxy/peanut structure (Dékány et al., 2013).

The main goal of GIBS is to couple chemical and kinematical information for 200–400 stars in each of 31 fields across the Bulge area in order to investigate whether we can confirm the presence of two distinct components, and what their properties are. The core of the project is the ESO Large Programme 187.B-0909 (PI: Zoccali), targeting red clump stars in 24 fields. These data complement other archival data acquired using the same GIRAFFE instrument setup, wavelength range and signal to noise (S/N). Specifically, we also analysed another 111 red clump stars in Baade's Window acquired within a pilot programme designed to build a calibration of Calcium II Triplet (CaT) equivalent widths versus $[\text{Fe}/\text{H}]$ (Programme 385.B-0735; Vásquez et al., 2015, in preparation). Another ~ 100 red clump stars in each of five fields at Galactic latitude, $b = -2^\circ$ were added from programme 089.B-0830 (PI: Gonzalez). Finally, we include in all the plots another 454 red clump stars in a field at $(l, b) = (0^\circ, -6^\circ)$ for which the CaT spectral region was measured with the Inamori Magellan Areal Camera and Spectrograph (IMACS)

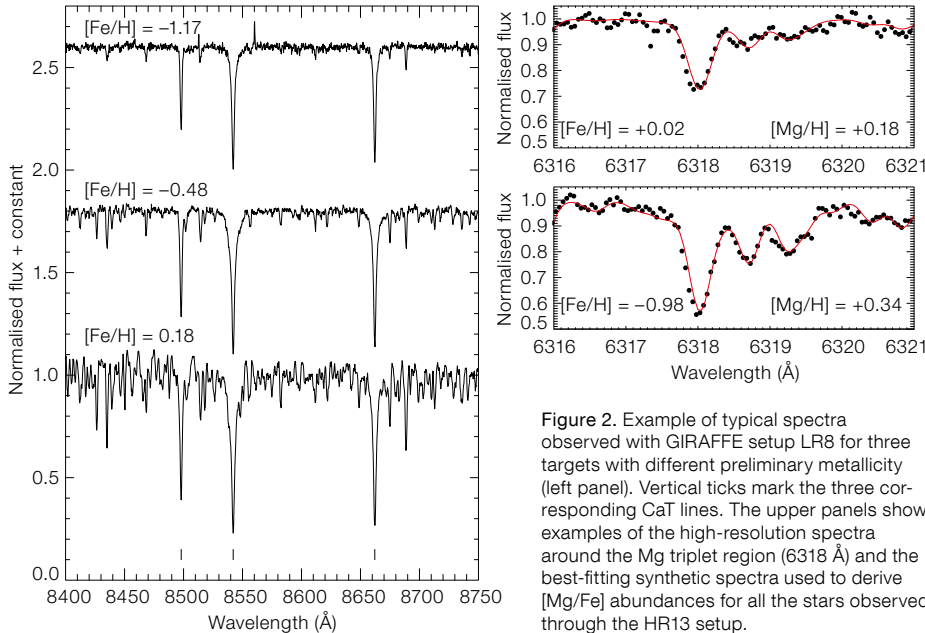


Figure 2. Example of typical spectra observed with GIRAFFE setup LR8 for three targets with different preliminary metallicity (left panel). Vertical ticks mark the three corresponding CaT lines. The upper panels show examples of the high-resolution spectra around the Mg triplet region (6318 Å) and the best-fitting synthetic spectra used to derive [Mg/Fe] abundances for all the stars observed through the HR13 setup.

spectrograph at the Magellan Telescope (Vázquez et al., 2013). Figure 1 shows the location of the 31 observed fields on an image of the Bulge.

All the spectra, with the exception of those in the fields at latitude -4° were obtained with the FLAMES GIRAFFE setup LR8, at a resolution $R = 6500$, centred on the CaT spectral feature at ~ 8500 Å. Their typical S/N, per pixel, is ~ 50 . About 200 stars were targeted in most of the fields, with the only exceptions being the fields along the Bulge minor axis, where spectra for ~ 400 stars were obtained. Stars in the fields at $b \sim -4^\circ$ were observed at a higher spectral resolution ($R = 22\,500$) with setup HR13, centred at ~ 6500 Å, in order to measure the chemical abundance of iron and the light elements, and to investigate the presence of radial gradients in the α -element ratios across different longitudes. The typical S/N per pixel of these high-resolution spectra is ~ 100 . Figure 2 shows sample spectra for stars of different metallicity taken with the two setups.

Radial velocities

Heliocentric radial velocities (RVs) were measured by cross-correlations using the IRAF *fxcor* task. For the low-resolution spectra the adopted template was a synthetic spectrum for stellar surface

parameters $T_{\text{eff}} = 4750$ K, $\log g = 2.5$ and $[\text{Fe}/\text{H}] = -1.3$. The template metallicity was chosen to be on the low side of the distribution in order to avoid including too many weak, unresolved lines. For the high-resolution, HR13 spectra, the cross correlation was performed with the same IRAF routine, but a template synthetic spectrum with $T_{\text{eff}} = 4500$ K, $\log g = 2.3$ and $[\text{Fe}/\text{H}] = -0.3$. The typical error on these velocities is ~ 0.6 km s^{-1} .

The GIBS survey allows the radial distribution of the inner Bulge regions ($b = -1^\circ, -2^\circ$) to be investigated for the first time; both are inaccessible to the Bulge Radial Velocity Assay survey (BRAVA; Rich et al., 2007) and the Abundances and Radial velocity Galactic Origins Survey (ARGOS; Freeman et al., 2013). Extensive discussion of the RVs is presented in Zoccali et al. (2014), including a comparison with previous works. We show in Figure 3 the observed mean RV and velocity dispersion in each field, together with the rotation profiles predicted by the boxy peanut bulge models by Martínez-Valpuesta et al. (2006). A remarkable agreement is apparent at all latitudes, except for the velocity dispersion profile at $b = -2^\circ$, where the data show a central peak not present in the models. The peak, visible in the third row, right panel of Figure 3, at $l = 0^\circ$, might be due to a high density peak in the inner ~ 250 pc, or perhaps to some anisotropy in the velocity distribution.

The general rotation pattern of the Bulge, together with the central peak in the velocity dispersion can both be appreciated much better in a kinematical map of the inner Galaxy, constructed by interpolating the data points shown in Figure 3. The map, shown in Figure 4, and discussed in Zoccali et al. (2014), can be directly compared with kinematical maps of external bulges of external galaxies from integral field unit (IFU) surveys such as, e.g., ATLAS^{3D} (Emsellem et al., 2004) and the Calar Alto Legacy Integral Field Area Survey (CALIFA; Sánchez et al., 2012). In addition, it provides the expected mean RV and velocity dispersion, σ , at any location within the area mapped by GIBS.

Metallicity distribution function across the inner Galactic Bulge

Iron abundances from GIRAFFE low-resolution spectra are obtained using CaT lines as a metallicity indicator. The correlation between the equivalent widths of CaT lines and global metallicity was first demonstrated in the late 1980s by means of integrated spectra of Galactic globular clusters. Later on this empirical evidence was confirmed in several studies of individual star spectra, and it has been extensively used in the study of Galactic star clusters and Milky Way satellites. Before starting the present programme we made sure that such a correlation would hold for super-solar metallicities, with the [Ca/Fe] profile appropriate for Bulge K giants. About 200 red clump and red giant branch stars were observed at both high resolution (HR13, HR14) and low resolution (LR8). These observations were used to derive a CaT versus [Fe/H] calibration specifically designed for the targets of the GIBS programme (Vázquez et al. 2015, in preparation).

For the stars observed at $R \sim 22\,500$, with the HR13 setup, metallicities and element ratios are derived using the same iterative method described in Zoccali et al. (2008) and Gonzalez et al. (2011). Specifically, equivalent widths of isolated Fe lines are obtained automatically by means of the DAOSPEC automated code. The list of lines is the same as that which was used in Zoccali et al. (2008) and Gonzalez et al. (2011),

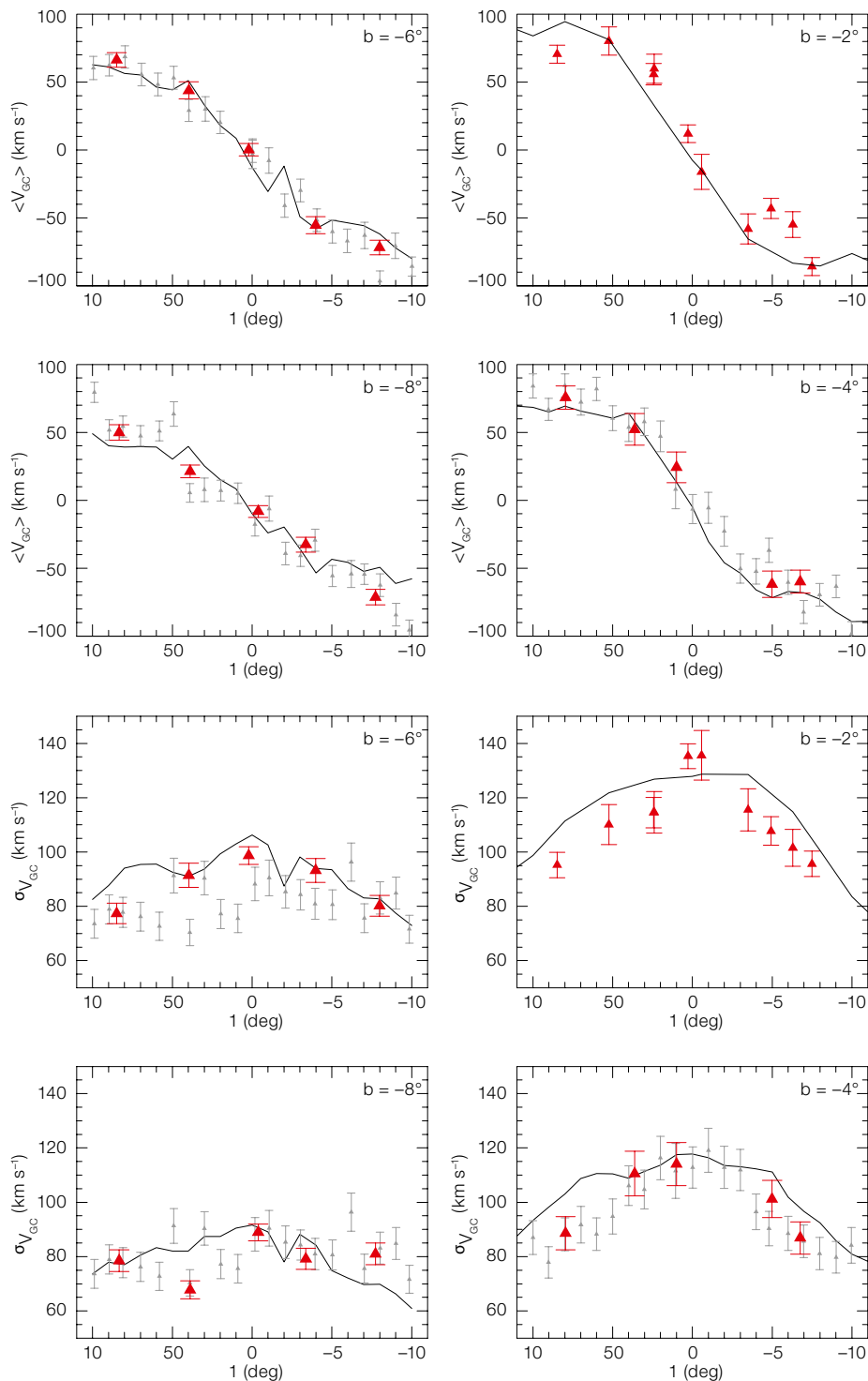


Figure 3. Mean galactocentric RV (upper four panels) and velocity dispersion (lower four panels) as a function of Galactic longitude for GIBS fields at different latitudes (red symbols) compared to the models by Martinez-Valpuesta et al. (2006; solid lines) at the same latitudes. Data for the BRAVA survey, when available, are also plotted in grey.

which was carefully calibrated to template stars μ Leonis, Arcturus and the Sun. First-guess photometric temperatures and gravity were obtained from the Optical Gravitational Lensing Experiment (OGLE-II) optical photometry, after

correcting for interstellar extinction using the map by Gonzalez et al. (2012). Surface gravity was derived photometrically as described in Zoccali et al. (2008). The first-guess parameters were used to create an ATLAS9 model atmosphere (Castelli & Kurucz, 2004). Effective temperature and micro-turbulent velocity were then spectroscopically refined by simultaneously imposing excitation equilibrium on a list of unblended Fe I and Fe II lines and by forcing a zero slope in the relation between equivalent widths and the derived abundance of each line. A new ATLAS9 model atmosphere was then generated using the new set of parameters and the procedure was repeated until the optimal set of parameters was found. The entire procedure was carried automatically for the entire high-resolution sample using the code GALA (Mucciarelli et al., 2013). Final metallicities were used to construct the metallicity distributions that are shown in Figure 5.

The derived metallicities allow us to explore by direct spectroscopic measurements the metallicity gradient along latitude and longitude in the inner Galactic Bulge. Figure 5 shows a subsample of 26 out of 31 fields following a regular grid, for a direct comparison of the metallicity distribution functions along longitude and latitude strips. The data clearly show a vertical gradient at each given longitude, which is consistent with the pattern derived from photometry using VVV data (Gonzalez et al., 2013). The spatial coverage of GIBS allows us to explore this gradient as close to the Galactic Plane as $b = -2^\circ$. Along the minor axis ($l = 0^\circ$) there is an extra field $b = -1^\circ$. The inner fields show a flattening of the vertical gradient close to the Plane, validating and extending the results by Rich et al. (2012) based on infrared spectroscopy of a few dozen stars along $l = 0^\circ$.

Chemical abundances

Using the spectroscopic stellar parameters, Ca and Mg abundances were calculated by means of fitting synthetic spectra to each observed spectrum of our sample. Synthetic spectra were created using the MOOG code fed by the corresponding MARCS model atmosphere and the line list from Gonzalez et al. (2011).

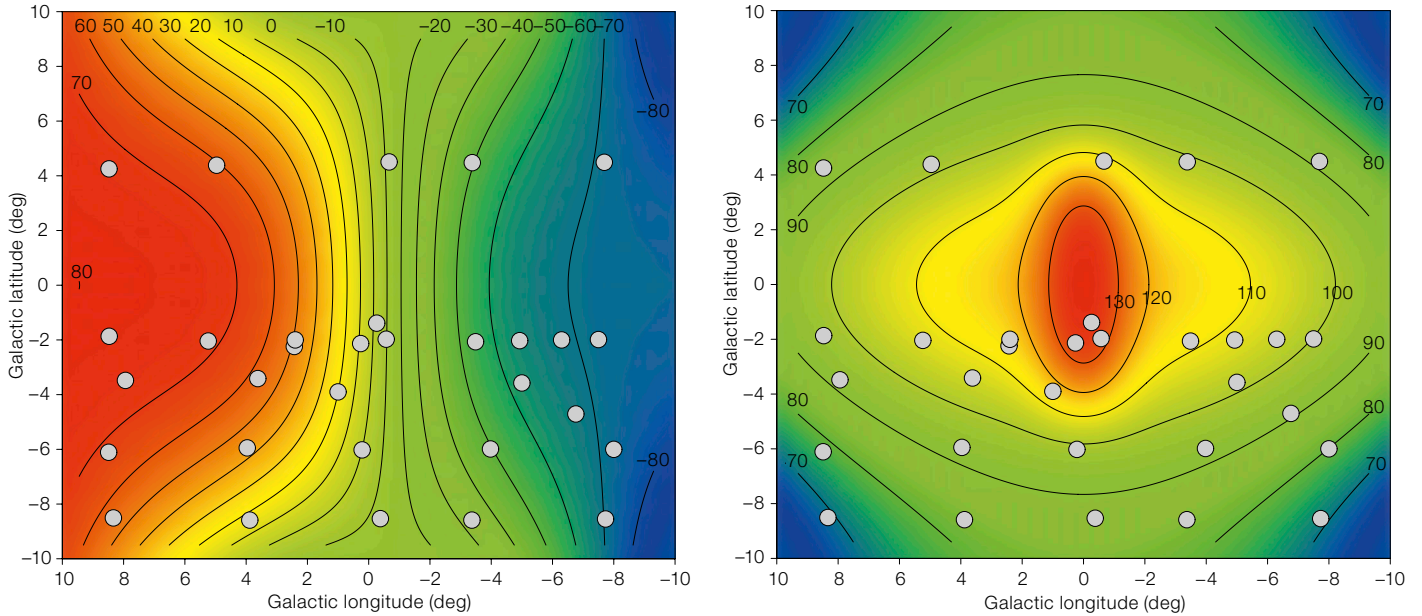


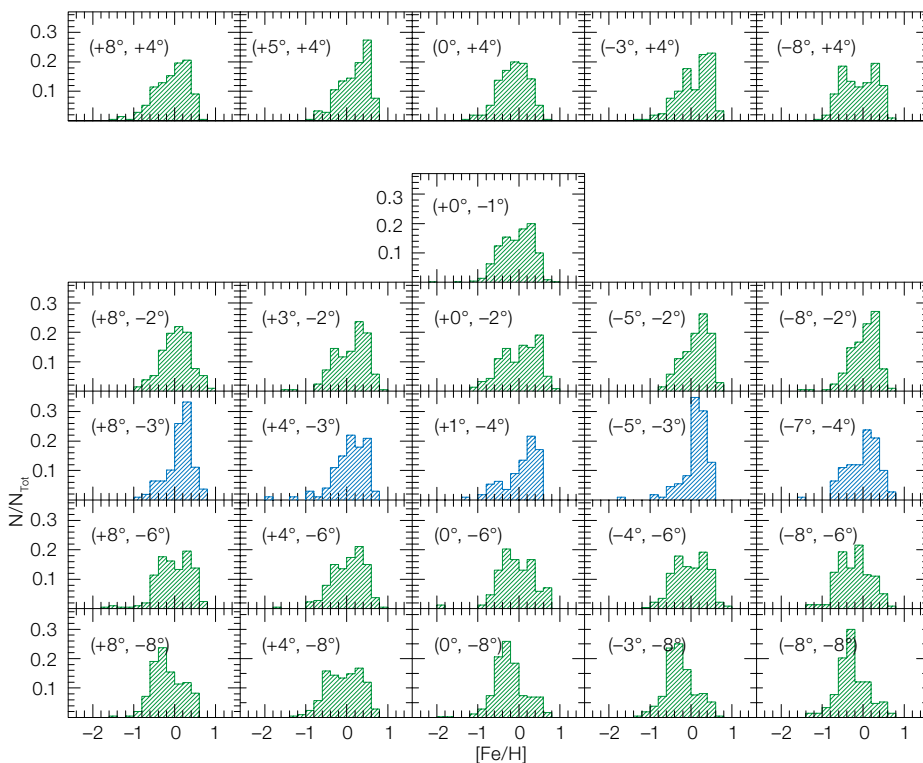
Figure 4. Mean radial velocity (left) and velocity dispersion (right) surfaces in the longitude–latitude plane, constructed from the measured rotation profiles at negative latitudes. Grey points show the positions of the GIBS 31 observed fields, while the black contour lines are labelled with the relevant velocity in km s^{-1} .

Figure 2 showed an example of the Mg region for a metal-poor and a metal-rich star in our sample and, in addition, the best-fit synthetic spectrum is also shown. Mg abundances derived in this way allow us to investigate the $[\text{Mg}/\text{Fe}]$ trend as a function of $[\text{Fe}/\text{H}]$, which is related to the

star formation timescale of a given stellar system. A high $[\text{Mg}/\text{Fe}]$ at a given $[\text{Fe}/\text{H}]$ indicates a rapid star formation. Figure 6 shows the $[\text{Mg}/\text{Fe}]$ trend for the entire GIBS high-resolution sample of Bulge red clump stars, together with the abundances for the sample of Bulge giants presented in Gonzalez et al. (2011). The smaller scatter in the GIBS data indicates the superior quality of the new data compared to previous ones. The higher S/N and a refined procedure to derive accurate stellar parameters have resulted in a fine set of measurements that will allow us to probe the Bulge abundance gradients with unprecedented accuracy. By comparing this relation to that of other Galactic components we are able to investigate the presence of chemical similarities/differences between the Bulge and the thin/thick Disc, and establish the relative star formation timescales (Gonzalez et al. 2015, in preparation).

The observations for the GIBS survey are currently complete. At least three major papers are about to be submitted, on the chemical abundances from the high-resolution spectra (as shown in Figure 6),

Figure 5. Metallicity distribution functions for a subsample of 26 fields along an approximately regular grid in Galactic coordinates (see labels). Metallicities measured from low- (green) and high- (blue) resolution GIRAFFE spectra are shown as dashed histograms.



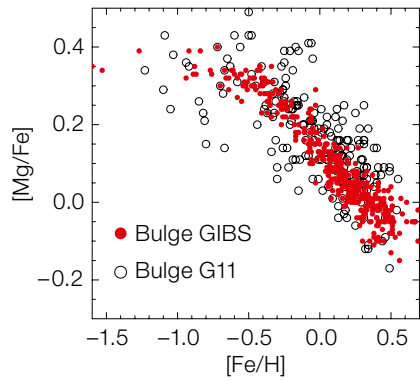


Figure 6. $[Mg/Fe]$ abundance ratios obtained from the HR13 spectra of 468 red clump stars in four GIBS fields (red), compared to those for red giant branch stars from the sample of Gonzalez et al. (2011; black symbols). See text for discussion.

the metallicity distribution function across all the fields (c.f., Figure 5) and a detailed analysis of the kinematics, from RVs and proper motions, coupled with metallicity. A further step includes tracing the oldest Bulge component, by means of RR Lyrae variables. Extensive catalogues of RR Lyrae stars are becoming available from the OGLE-IV survey in the optical (Soszynski et al., 2014) and the VVV survey in the near-infrared. A VIMOS spectroscopic programme aimed at deriving the radial velocity distribution of RR Lyrae stars in some inner Bulge fields has been awarded time for our group in Period 95.

References

- Blitz, L. & Spergel, D. N. 1991, *ApJ*, 379, 631
 Castelli, F. & Kurucz, R. F. 2004, *astro-ph/0405087*
 Dékány, I. et al. 2013, *ApJ*, 776, L19
 Emsellem, E. et al. 2004, *MNRAS*, 352, 721
 Freeman, K. et al. 2013, *MNRAS*, 428, 3660
 Gonzalez, O. A. et al. 2011, *A&A*, 530, A54
 Gonzalez, O. A. et al. 2012, *A&A*, 543, A13
 Gonzalez, O. A. et al. 2013, *A&A*, 552, A110
 Hill, V. et al. 2011, *A&A*, 534, A80
 Howard, C. D. et al. 2009, *ApJ*, 702, L153
 Martínez-Valpuesta, I. et al. 2006, *ApJ*, 637, 214
 Minniti, D. et al. 2010, *New Astronomy*, 15, 433
 Mucciarelli, A. et al. 2013, *ApJ*, 766, 78
 Rich, R. M. et al. 2007, *ApJ*, 658, L29
 Rich, R. M. et al. 2012, *ApJ*, 746, 59
 Sánchez, S. F. et al. 2012, *A&A*, 538, 8
 Soszynski, I. 2014, *Acta Astronomica*, 64, 177
 Vásquez, S. et al. 2013, *A&A*, 555, A91
 Zoccali, M. et al. 2014, *A&A*, 562, A6

ESO/VVV Team/A. Guzmán



The Galactic Plane star-forming region associated with IRAS 16562-3959 is shown in a VISTA *JHKs* colour image. The central source of this embedded and molecular region contains the high-mass ($\sim 15 M_{\odot}$) young stellar object G345.4938+01.4677. This luminous source is situated in a molecular rotating disc and has an outflow with an ionised jet. See Picture of the Week potw1448 for details.